Spring 2022

Automatic sparse esm scan using Gaussian process regression

Jiangshuai Li

Department:

AUTOMATIC SPARSE ESM SCAN

USING GAUSSIAN PROCESS REGRESSION

by

JIANGSHUAI LI

A THESIS

Presented to the Faculty of the Graduate School of the

MISSOURI UNIVERSITY OF SCIENCE AND TECHNOLOGY

In Partial Fulfillment of the Requirements for the Degree

MASTER OF SCIENCE IN ELECTRICAL ENGINEERING

2022

Approved by:

Daryl G Beetner, Advisor
Victor Khilkevich
DongHyun Kim

PUBLICATION THESIS OPTION

This thesis consists of the following two articles, formatted in the style used by the Missouri University of Science and Technology:

Paper I: Pages 3-18 have been published by 2020 IEEE International Symposium on Electromagnetic Compatibility & Signal/Power Integrity (EMCSI).

Paper II: Pages 19-38 have been published by 2021 IEEE International Symposium on Electromagnetic Compatibility & Signal/Power Integrity (EMCSI).

ABSTRACT

Emission source microscopy (ESM) technique can be utilized for localization of electromagnetic interference sources in complex and large systems. In this work a Gaussian process regression (GPR) method is applied in real-time to select sampling points for the sparse ESM imaging using a motorized scanner. The Gaussian process regression is used to estimate the complex amplitude of the scanned field and its uncertainty allowing to select the most relevant areas for scanning. Compared with the randomly selected samples the proposed method allows to reduce the number of samples needed to achieve a certain dynamic range of the image, reducing the overall scanning time. Results for simulated and measured 1D scans are presented.

This method allowed to reduce the number of samples needed to achieve a certain dynamic range of the image, reducing the overall scanning time and eliminating a need of human intervention into the ESM process. Based on the work of 1D scan and Gaussian Regression Sparse ESM strategy, the second work in this paper extends the application of the ESM with GPR sampling to 2D scenes with multiple sources, including distributed ones.

The automatic GPR ESM method can intelligently and automatically control the scanning process, reducing the number of measurement points with less image quality degradation compared to the random ESM scanning.

ACKNOWLEDGMENTS

I wish to express my thanks for the supports of Dr. Beetner, Dr. Victor, and Dr. Kim for this research., to the entire EMCLAB family, and to Missouri University of Science and Technology.

During my most tough stage where I lacked confidence and hope in pursuing my degree in the lab, it is Dr. Beetner who rescued me from the fire pit, rein in the cliff. Without him I could have not consisted in and accomplished my engineering dream.

Dr. Beetner built my personality and shaped me to be a human who bravely takes responsibility for the society and becomes self-motived in every obstacle through the life. Dr. Khilkevich, a taciturn professor, who knocked on and open the slice of the scientific and mathematic door for me, spared no effort in guiding and teaching me from scratch; under his selfless cultivation, I can dive into the vast ocean of engineers, frivolous, and tireless. Left blooming alone, no flower of her kindred; who would inhabit this bleak world alone. No one parsed and is able to.

'I heard the echo, from the valleys and the heart, open to the lonely soul of sickle harvesting, repeat outrightly, but also repeat the well-being of eventually swaying in the desert oasis'.

TABLE OF CONTENTS

Page

LIST OF ILLUSTRATIONS

LIST OF TABLES

1. INTRODUCTION

Electromagnetic emission has been receiving increasing attention to the rapid growth of the electronic industry. Consequently, electronic equipment and systems become more susceptible to electromagnetic interference (EMI). To deal with the electromagnetic interference (EMI) caused by the noise, it is of critical importance to identify the emission sources. In complex electronic systems, noise is a product of multiple, often uncorrelated, emission. In a situation with multiple sources knowing the contributions of the individual sources might help to solve the emission problems.

Near-field scanning (NFS) is a widely used technique to characterize and localize the radiation sources in the complex electronic environment accurately and reliably. The NFS measurements can be used to estimate the far-field pattern and identify the radiating sources with the assistance of the emission source microscopy (ESM) technique. However, due to the increased functionality and the circuit density of the electronic devices, it is usually hard to resolve the individual radiating sources with the help of NFS if the phase information is missing. Therefore, the ability to measure the amplitude and the phase of the electromagnetic fields is of critical importance.

A method that uses two moving probes for NFS has been developed for complete characterization of stochastic fields (the phase information is contained in the spatial correlation function of the fields), which is, however, very time consuming and requires large computational resources.To reduce the measurement time and to avoid measuring spatial correlations, a signal resolving method was proposed which requires placing reference probes near the actual sources of radiation and canceling contributions of all

other sources. Another critical EMC measurement is total radiated power. In many circumstances, the electronic equipment may be extremely complicated or compact such that it is difficult or impossible to place the reference probe close to the radiation sources. A new method is proposed in this paper so that all probes can be placed far away from the sources such that no access to the sources to obtain the reference signals is required. The complexity of the measurement and data processing time are consequently reduced.

In Paper I, a method for the total radiated power measurement of multiple non-correlated emission sources in the reverberation tent is proposed. Reverberation chambers, in general, are widely used as established environments to perform electromagnetic susceptibility and emission measurements . A well-stirred reverberation chamber emulates a statistically uniform and isotropic field within its working volume, providing a simple, cheap, and effective way to measure the total radiated power.

In order to resolve the contributions of the individual sources in the multi-sourced environment, a BSS-based method is introduced. Blind source separation deals with recovering a set of underlying sources from an unknown mixture.

Application of the BSS to separate signals in a conventional reverberation chamber with the discrete and well-controlled movement of the stirrer is straightforward (since for each position of the stirrer, the chamber represents a time-invariant system). However, in recent years, reverberation tents are gaining popularity due to their low cost and ease of use. In the reverberation tents, the mode stirring is performed by random shaking of the tent's walls, and the entire measurement setup is inherently time-variant. The intent of this paper is to investigate the possibility of using BSS to separate signals and eventually measure their TRP contributions in a reverberation tent.

PAPER

I. AUTOMATIC SPARSE ESM SCAN USING GAUSSIAN PROCESSREGRESSION

Jiangshuai Li, Jiahao Zhou, Shaohui Yong, Yuanzhuo Liu, Victor Khilkevich

EMC Laboratory, Missouri University of Science and Technology
Rolla, MO, USA

ABSTRACT

Emission source microscopy (ESM) technique can be utilized for localization of electromagnetic interference sources in complex and large systems. In this work a Gaussian process regression (GPR) method is applied in real-time to select sampling points for the sparse ESM imaging using a motorized scanner. The Gaussian process regression is used to estimate the complex amplitude of the scanned field and its uncertainty allowing to select the most relevant areas for scanning. Compared with the randomly selected samples the proposed method allows to reduce the number of samples needed to achieve a certain dynamic range of the image, reducing the overall scanning time. Results for simulated and measured 1D scans are presented.

1. INTRODUCTION

Emission source microscopy (ESM) is a technique that can localize and characterize radiation sources in complex systems by measuring the electromagnetic field

magnitude and phase over the planar surface at a typical distance of several wavelengths away from the DUT [1].

Uniform ESM imaging provides the best results in terms of the image quality [2], but leads to a long scanning time needed to sample the fields on the plane with sub-wavelength step required to satisfy the Nyquist criterion. To overcome the problem a sparse scanning strategy was proposed [3]. As [4] demonstrates, with the random selections of the sampling locations, the dynamic range of the image (related to the amount of noise added due to space sampling) is equal to the number of samples. And while sparse random sampling often produces satisfactory results, it still can lead to prohibitively long scanning times needed to achieve a desirable image quality. An alternative to random sampling is manual sampling [3], [5] which usually provides fast scanning but requires a human operation, and the scanning process is affected by operator's subjective decisions and perceptions. This paper proposes an automated method to select the sampling points based on the Gaussian process regression, eliminating a need of human intervention into the ESM process.

Gaussian process regression (GPR) can predict the field distribution based on randomly and sparsely measured samples. In this study, the Gaussian process regression is applied to select the next scanning location based on the previous ones. The automatic GPR ESM method can intelligently and automatically control the scanning process, reducing the number of measurement points with less image quality degradation compared to the random ESM scanning.

The paper is organized as follows. Section II introduces the sparse ESM technique and Gaussian process regression. In Section III the system setup of sparse ESM using

Gaussian process regression is illustrated, and the simulation and measurement results are demonstrated. Finally, the summary is given.

2. SPARSE ESM AND GAUSSIAN PROCESS REGRESSION

2.1. OVERVIEW OF SPARSE ESM TECHNIQUE

The ESM algorithm is based on the synthetic aperture radar technique, which uses the two-dimensional (2-D) Fourier transformation. The field (image) on the DUT plane after back-propagation can be expressed as follows:

$$E_t^0(x, y, 0) = \mathcal{F}^{-1}\{\mathcal{F}[E_t(x, y, z_0)] \cdot e^{jk_z z_0}\}, \tag{1}$$

where

$$k_z = \sqrt{k^2 - k_x^2 - k_y^2}, \text{ if } k_x^2 + k_y^2 \leq k^2,$$

$$k_z = -j\sqrt{k^2 - k_x^2 - k_y^2}, \text{ otherwise.} \tag{2}$$

In (2) k is the wave number, and k_x, k_y, k_z are the components of the propagation vector (or the spatial frequencies in x-, y-, and z- directions). $E_t(x, y, z_0)$ is the tangential fields on the scanning planar surface (x, y) at the elevation z_0 above the image plane (see. Figure 1). The ESM system is consist of the scanning plane, the imaging plane, and the probe antenna which is applied to scanning the radiation power over the DUT in the scanning plane.

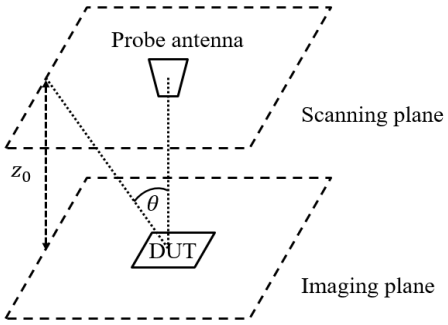

Figure 1. 2-D ESM scanning arrangement.

Since the sparse ESM is carried out with non-uniform scanning points, a predefined grid of zero values is created before the scanning and filled-in during the scanning process [2], [4]. The zero-valued grid should be defined with a step size much smaller than the wavelength to minimize the phase errors in the field caused by the difference of the actual and discretized locations of the probe. For example, when working at 3 GHz, the reasonable choice of the step could be 2 mm (12.5 points per wavelength), which could cause a relatively small phase as well as localization errors. At the same time the zeros in the scanned field distribution lead to noise in the image. The signal-to-noise ratio of the acquired image is approximately equal to the number of the sparse samples and does not depend on the density of the grid [4].

2.2. INTRODUCTION OF GAUSSIAN PROCESS REGRESSION

A Gaussian process is a collection of random variables, any finite number of which have a joint Gaussian distribution [6]. A Gaussian process is completely specified by its mean value

$$\mu(w) = \mathbb{E}[(w)], \tag{3}$$

where w is the input vector (sampled function) and $\mathbb{E}$ is the expected value operator, and a covariance function：

$$k(w, w') = \mathbb{E}\big[\big(f(w) - \mu(w)\big)\big(f(w') - \mu(w')\big)\big]. \quad (4)$$

Thus the Gaussian process can be written as：

$$f(w) \sim GP\big(\mu(w), k(w, w')\big), \quad (5)$$

where $f(w)$ is the estimated probability density of the process w, characterized by its mean value and covariance, and GP is the Gaussian process distribution.

Application of the GPR approximation is illustrated in Figure 2. A certain function (the curve "Actual" in the figure) is sampled at several locations (marked by crosses). Application of the GPR allows to estimate the mean value of the function ("μ") and its uncertainty (or the confidence interval "$\mu + \sigma$" and "$\mu - \sigma$").

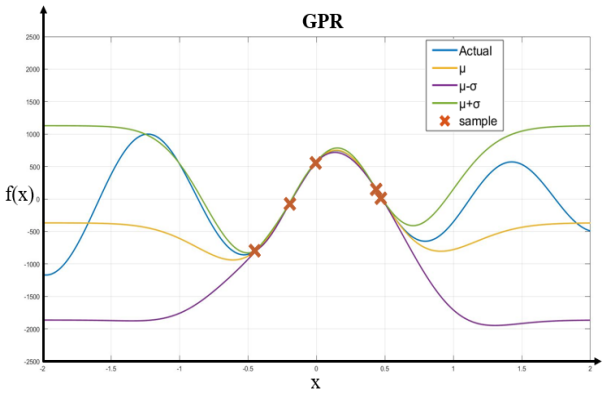

Figure 2. An example of a 1D GPR estimation.

The results of the GPR can be regarded as the fit of the function $f(x)$ with the provided fit uncertainty. As can be seen from the example, the function $f(x)$ is well fitted

at the interval from approximately -0.5 to 0.5 (this interval is characterized by small predicted uncertainty), and it is reasonable to add the consecutive sampling points outside this interval where the predicted uncertainty is large.

To perform the GPR fit the Matlab implementation of the Gaussian process regression is used throughout the rest of the paper. The main parameter needed to perform the GPR is the minimum value of the standard deviation σ_{min}. This value is important because it allows to set the "size" of the features that are supposed to be fitted by the GPR. If the minimum sigma value is too large, the function could be approximated by a constant (the variations of the function would be within the $\pm\sigma_{min}$ band relative to the constant). If the minimum value is too small, the GPR would try to fit measurement errors (such as additive noise), which is undesirable. The choice of the minimum value of sigma is an important problem, which requires additional investigation. In the presented implementation the minimum value of sigma was selected empirically.

2.3. SPARSE ESM SYSTEM USING GPR

The GPR is performed separately for real and imaginary parts of the measured field distribution. As the result of the GPR, the mean values μ_{real} and μ_{imag} as well as the standard deviations σ_{real} and σ_{imag} are estimated (all of these quantities are functions of the spatial coordinates on the sampling plane or line). The total field power and its uncertainty are then calculated as

$$P = \mu_{real}^2 + \mu_{imag}^2 , \tag{6}$$

$$\sigma = \sqrt{\sigma_{real}^2 + \sigma_{imag}^2} . \tag{7}$$

Obviously the regions with the largest power on the scan plane contribute the most to the ESM image. At the same time the large uncertainty in estimated field distribution leads to the large uncertainty in the image. So it is reasonable to scan primarily at the regions with high estimated power and high uncertainty. To satisfy these two requirement and empirical criterion was developed. According to it the next measurement is performed at the location x_{n+1} (n being the number of previously acquired samples) with the maximum product of the predicted power and uncertainty. At the same time, the next measurement point should not be closer than a certain distance ε (typically a fraction of a wavelength) to already sampled ones x_i to avoid undesirable clustering effect (see [2] for details):

$$x_{n+1} = x|\max[\sigma \cdot P],$$
$$\forall\, i \in [1\,, n\,]\,, |x_{n+1} - x_i| \geq \varepsilon. \tag{8}$$

The GPR fit can be performed if at least two samples are available. In the proposed implementation the first two initial samples are taken at random locations. The complete flow diagram of the process is shown in Figure 3.

Because of the constrain in (8), the distance between the sampling points cannot be smaller than ε, which allows to have only a limited number of samples in the scanning area. This leads to the natural stop of the algorithm when no more sampling points can be added.

The ESM imaging can be performed periodically during the scan to observe image evolution in real time, or after the stop of the algorithm.

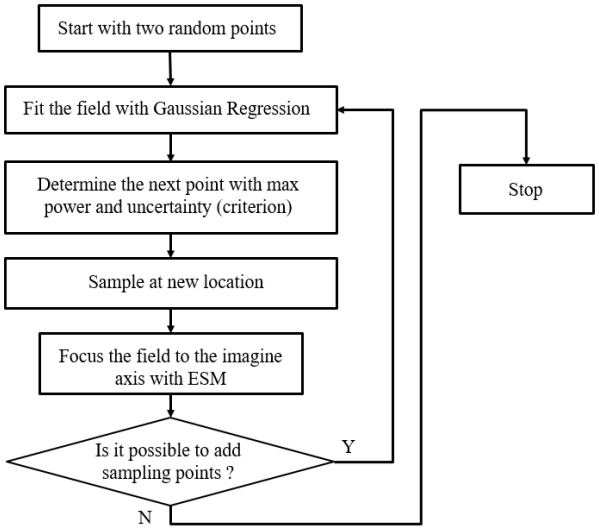

Figure 3. Flow diagram of real-time automatic ESM using GPR.

3. SIMULATION AND MEASURMENT REULTS

3.1. SIMULATION RESULT (1D)

In the simulation of the automatic sparse ESM using Gaussian process regression, three horizontally oriented dipoles are put on the image line at different positions. The working frequency is 10 GHz, with the wavelength λ=0.03 m, and the length of the scanning and image lines is 20 λ (0.6 m). The E_x (tangential) component of the field due to the dipoles was calculated on the scan line using analytical formulas for an infinitesimal dipole [7]. The parameters of the dipoles are listed in Table 1.

To verify the performance of the GPR method, the random sampling method is simulated as a comparison. The images obtained as the result of the ESM process are normalized to their corresponding maxima to facilitate their comparison (the absolute values of the images depend on the number of samples and the sampling step).

Table 1. Parameters of radiation sources used in simulation.

Source	Dipole 1	Dipole 2	Dipole 3
Position [λ]	-8	1	5
Dipole moment [A·m]	0.01	1	1

Estimation of the absolute value of the image can be performed using interpolation of the scanned field as described in [4]. Accuracy of this process with respect to the GPR imaging requires additional investigation.

To quantify the error of the obtained image the mean squared difference between the normalized images is calculated:

$$MSE_E = \frac{1}{m}\sum_{i=1}^{m}\left(\frac{|E_S(i)|}{\max|E_S|} - \frac{|E_0(i)|}{\max|E_0|}\right)^2, \quad (9)$$

where E_S is the image obtained by using the GPR or the random sampling method, E_0 is the actual image (complete uniform scan), and m is the number of the samples in the image (i.e. the on the samples in the predefined grid).

The images obtained by taking 120 samples randomly or by the GPR selection with comparison to the actual image are show in Figure 4 (a). As can be seen, even with this relatively low number of points the GPR sampling allows to resolve the weak source (dipole 1), while in the image obtained by the random sampling, the weak source cannot be identified because of high level of noise. The evolution of the mean squared error in the scanning process is illustrated by Figure 4(b).

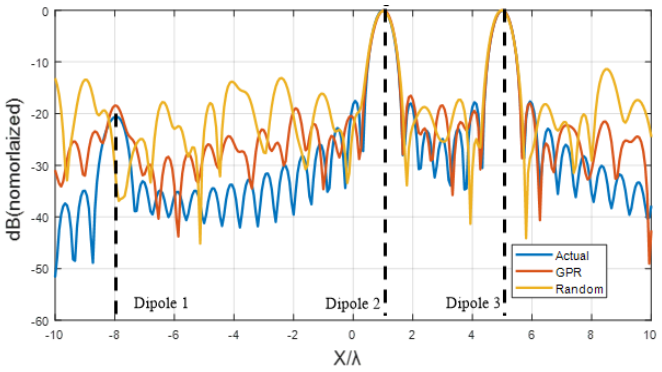

(a)

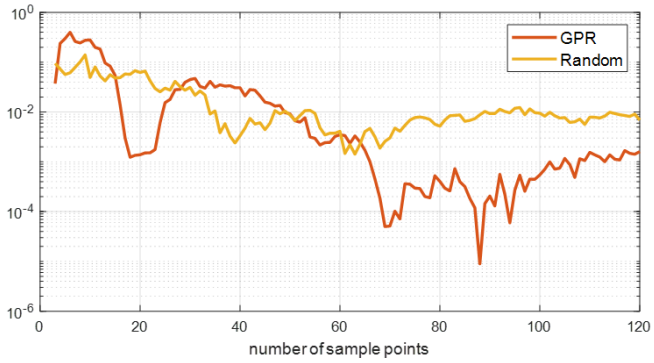

(b)

Figure 4. Images obtained by GPR and random sampling:
ESM image with 120 measured samples (a), the MSE_E as a function of the number of sampling points (b).

As can be seen, the accuracy of the GPR imaging (characterized by the corresponding MSE value) is consistently better than that of the random sampling starting from approximately 70 acquired samples and after 120 iterations the error in the GPR imaging error is approximately 10 times lower than that of the random scanning process. Both plots in Figure 4 demonstrate the advantage of the GPR imaging over random sampling in terms of the scanning time – i.e. the ability to obtain the image of better quality for the same number of acquired samples, or to reduce the number of samples needed to obtain an image of a certain quality.

3.2. MEASUREMENT RESULT (1D)

The scanning system setup is illustrated in Figure 5. The scanning probe is attached to the carriage that can move on a frame. The carriage is moved by two stepper motors with two timing belts. The Microcontroller Unit (MCU) receives commands from the PC and controls the stepper motors.

The DUT on the image plane and the probe on the scanning plane are both log-periodic antennas with the working frequency range of 850-6500MHz. The antennas are connected to the VNA ports. By measuring the transmission coefficient (S_{21}) between the antennas it is possible to measure the complex values of the field amplitude at the scanning antenna location (scaled by the unknown, but irrelevant in this case, antenna and cable factors). The measured component is determined by the orientation of the scanning log-periodic antennas (x or y).

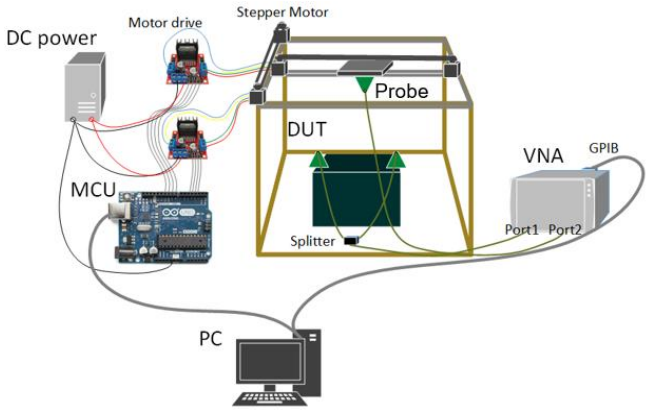

Figure 5. Automatic sparse ESM system setup.

The scanner allows to perform 2D scans, but only 1D scan results are reported in this paper. Implementation of the 2D scanning with the GPR is subject of the ongoing work.

In the 1D scans only one motor of the scanner is engaged and the scanning is performed along the line over the DUT (Figure 6). In the scanning process the predefined zero-valued array is filled with the sampled field values. The extent of the scan range is 0.6 m with 6001 pre-defined sampling locations, resulting in the sampling step of 0.1 mm. The measurements are performed at 3 GHz.

Figure 6 illustrates the source arrangement. Two antennas are placed on the focus line at locations -0.2 m and 0.1 m (0 corresponds to the center of the scan line); the distance between the focus line and the scanning axis is 0.4 m. The two source antennas are connected to the VNA through a splitter, providing roughly equal excitation. By measuring the S_{21} between the VNA ports, the field on the scanning axis is obtained. Similar with the simulated results presented in the previous section, uniform, random, and GPR sampling measurement were performed.

The total number of sampling points of the uniform sampling measurement was 241 (sampling step was 2.5 mm corresponding to 40 samples per wavelength. Next two figures illustrate the convergence process during the GPR scan. Figure 7 (a), (b) show the fit of the real and imaginary parts of the field after 10 acquired samples. As can be seen, the GPR instructed the scanner to scan primarily over source 2, where the field is already collected with relatively high density and accuracy.

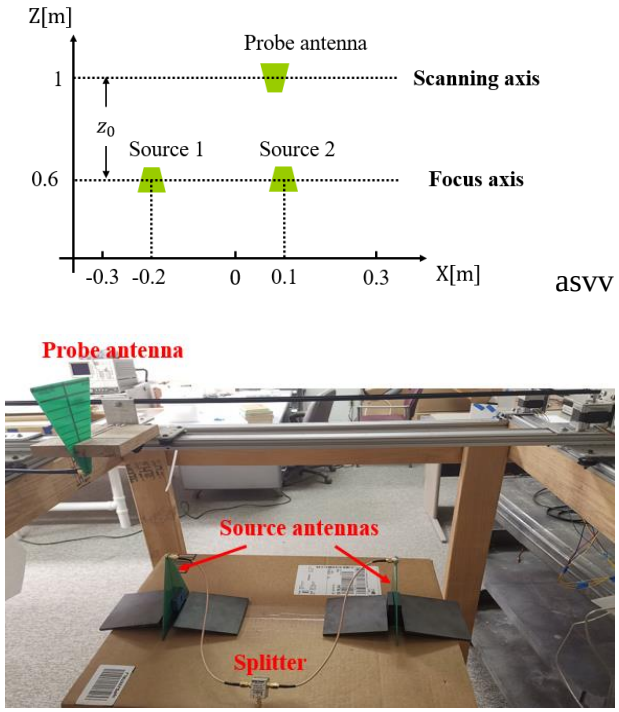

Figure 6. Measurement setup geometry and photo.

Figure 7 (c) shows the curves related to the criterion (8), and Figure 7 (d) demonstrated the image obtained after collecting 10 samples in comparison to the reference (result of the uniform scan).

After 10 samples the images already start to reveal two peaks corresponding to two sources, and while the image quality is low in both GPR and random cases, the GPR image is already closer to the reference (uniform scan) than the random scan image. Figure 8 demonstrates the results at 100^{th} iteration (close to the end of the GPR scan process), showing convergence of the GPR and the random sampling images to the reference.

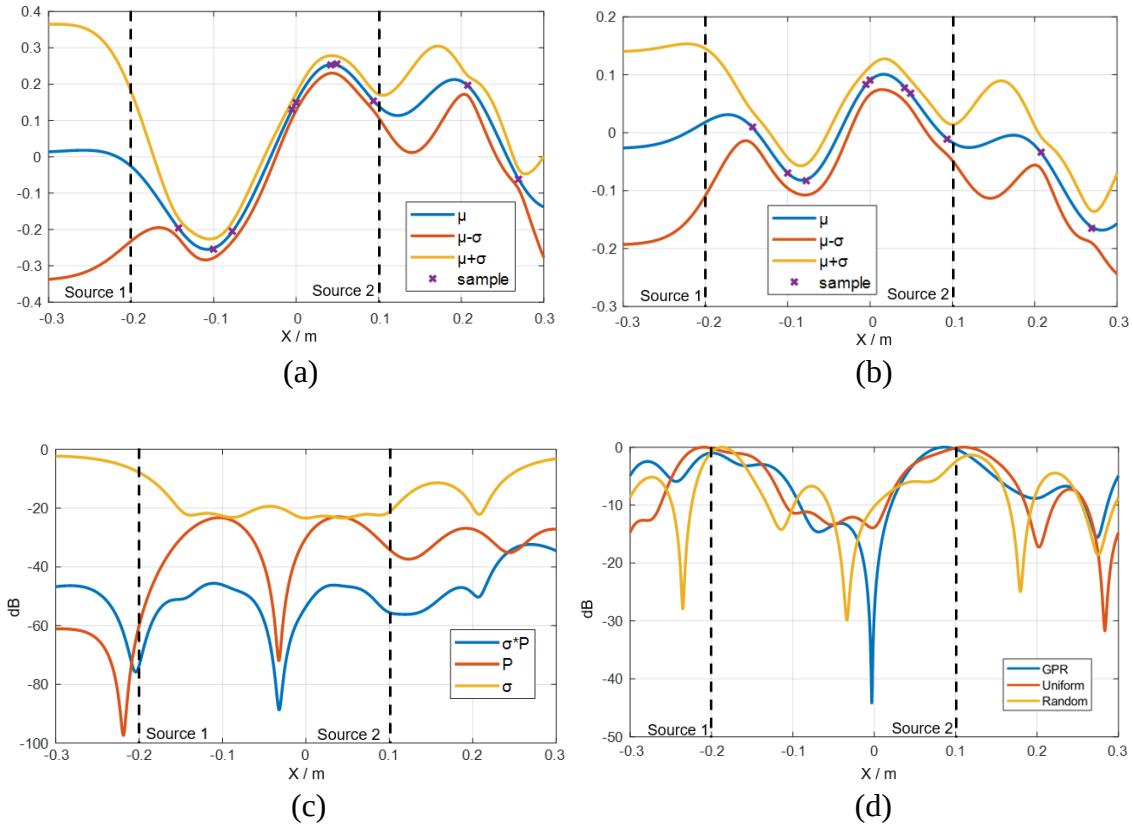

Figure 7. GPR ESM scanned field and ESM image obtained after 10 samples : predicted real part (a), predicted imaginary part (b), predicted power and uncertainty (c), ESM images for GPR,uniform, and random scanning (d).

As can be seen, the GPR sampling points cover the scan line almost uniformly; however, the samples are not collected around points $x = -0.03$ m, $x = -0.18$ m, and $x = 0.13$ m which correspond to the nulls of the field power, demonstrating intelligent scan point selection. After 100 sampling the image obtained by the GPR scanning is significantly better than that obtained by the random scan (Figure 8 (d)).

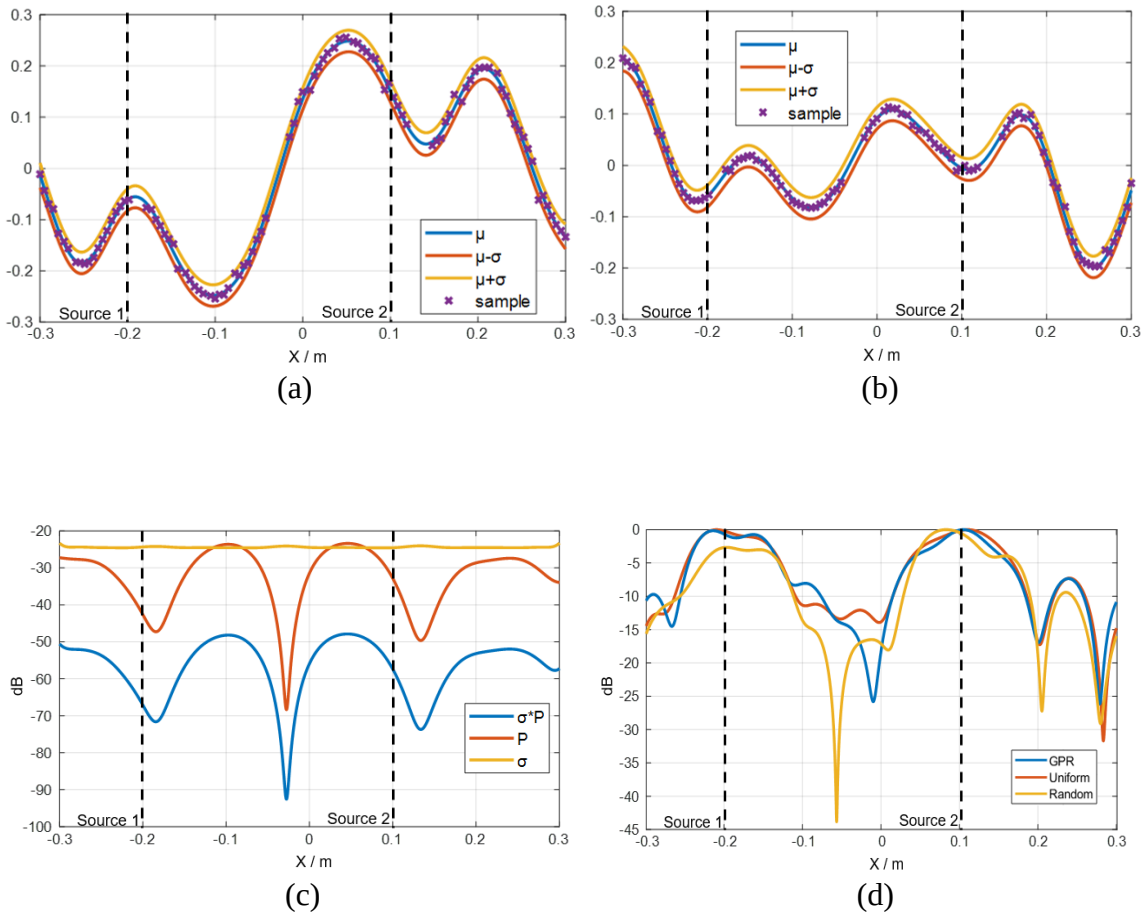

Figure 8. GPR ESM scanned field and ESM image obtained after 100 samples: predicted real part (a), predicted imaginary part (b), predicted power and uncertainty (c), ESM images for GPR, uniform, and random scanning (d).

4. SUMMARY

An automatic sparse ESM using Gaussian process regression method has been developed. Using the proposed method, the quality of the ESM imaging can be improved compared to the random scan without using operator-controlled setup. The number of the scan points can be potentially reduced compared to uniform and random scan due to intelligent selection of scan areas relevant for the image.

REFERENCES

[1] P. Maheshwari, H. Kajbaf, V. V. Khilkevich, and D. Pommerenke, “Emission source microscopy technique for EMI source localization,” IEEE Trans. Electromagn. Compat., vol. 58, no. 3, pp. 729–737, Jun. 2016.

[2] M. Sørensen, H. Kajbaf, V. V. Khilkevich, L. Zhang and D. Pommerenke, "Analysis of the Effect on Image Quality of Different Scanning Point Selection Methods in Sparse ESM," in IEEE Transactions on Electromagnetic Compatibility, vol. 61, no. 6, pp. 1823-1831, Dec. 2019.

[3] J. T. Case, M. T. Ghasr, and R. Zoughi, “Nonuniform manual scanning for rapid microwave nondestructive evaluation imaging,” IEEE Trans. Instrum. Meas., vol. 62, no. 5, pp. 1250–1258, May 2013.

[4] L. Zhang, V. Khilkevich and D. Pommerenke, "Sparse Emission Source Microscopy for Rapid Emission Source Imaging," in IEEE Transactions on Electromagnetic Compatibility, vol. 59, no. 2, pp. 729-738, April 2017.

[5] H. He, V. Khilkevich and D. Pommerenke, "2D imaging system with optical tracking for EMI source localization," 2015 IEEE Symposium on Electromagnetic Compatibility and Signal Integrity, Santa Clara, CA, 2015, pp. 107-110.

[6] [6]. C. E. Rasmussen & C. K. I. Williams, Gaussian Processes for Machine Learning, the MIT Press, 2006, ISBN 026218253X. © 2006 Massachusetts Institute of Technology.

[7] C. A. Balanis, Antenna Theory: Analysis and Design, New York:Wiley, 1982.

II. IMAGING DISTRIBUTED SOURCES WITH SPARSE ESM TECHNIQUE AND GAUSSIAN PROCESS REGRESSION

Jiangshuai Li , Victor Khilkevich , Ruijie He, Yuanzhuo Liu, Jiahao Zhou

EMC Laboratory, Missouri University of Science and Technology
Rolla, MO, USA

ABSTRACT

Emission source microscopy (ESM) technique can be utilized for the localization of electromagnetic interference sources in complex and large systems. In this work, a Gaussian process regression (GPR) method is applied in real-time to select sampling points for the sparse ESM imaging. The Gaussian process regression is used to estimate the complex amplitude of the scanned field and its uncertainty allowing to select the most relevant areas for scanning. Compared with the random selection of samples the proposed method allows to reduce the number of samples needed to achieve a certain dynamic range of the image, reducing the overall scanning time. Results for simulated and measured 2D scans for multiple and distributed emission source are presented.

1. INTRODUCTION

Emission source microscopy (ESM) is a technique that can localize and characterize radiation sources in complex systems by measuring the electromagnetic field magnitude and phase over the planar surface at a typical distance of several wavelengths away from the device under test (DUT) [1].

Uniform ESM imaging provides the best results in terms of the image quality, but leads to a long scanning time needed to sample the fields on the plane with sub-wavelength step required to satisfy the Nyquist criterion [2]. To overcome the problem a sparse scanning strategy was proposed [4]. As [4] has demonstrated, with the random selection of the sampling locations, the dynamic range of the image (related to the amount of noise added due to space sampling) is equal to the number of samples. And while sparse random sampling often produces satisfactory results, it still can lead to prohibitively long scanning times needed to achieve a desirable image quality. An alternative to random sampling is manual sampling [3], [5] which usually provides fast scanning but requires a human operation, and the scanning process is affected by the operator's subjective decisions and perceptions. In recent years the Gaussian process regression (GPR) or Kriging interpolation was proposed as a method for fast scanning of electromagnetic fields [6, 7]. In [8] the GPR strategy was successfully applied to the ESM scan. This method allowed to reduce the number of samples needed to achieve a certain dynamic range of the image, reducing the overall scanning time and eliminating a need of human intervention into the ESM process. However, in [8] only 1D scans with a maximum of two point sources were performed. This paper extends the application of the ESM with GPR sampling to 2D scenes with multiple sources, including distributed ones.

In this study, the Gaussian process regression is applied to select the next scanning location based on the previous ones. The automatic GPR ESM method can intelligently and automatically control the scanning process, reducing the number of measurement points with less image quality degradation compared to the random ESM scanning.

The paper is organized as follows. Section II introduces the sparse ESM technique and sparse ESM system using GPR. In Section III the system setup of sparse ESM using Gaussian process regression is illustrated and the simulation and measurement results are demonstrated. Finally, the summary is given.

2. SPARSE ESM AND GAUSSIAN PROCESS REGRESSION

2.1. OVERVIEW OF SPARSE ESM TECHNIQUE

The ESM algorithm is based on the synthetic aperture radar technique, which uses the two-dimensional (2-D) Fourier transform. The field (image) on the DUT plane after back-propagation can be expressed as follows:

$$E_t^0(x, y, 0) = \mathcal{F}^{-1}\{\mathcal{F}[E_t(x, y, z_0)] \cdot e^{jk_z z_0}\}, \tag{1}$$

where

$$k_z = \sqrt{k^2 - k_x^2 - k_y^2}, \text{ if } k_x^2 + k_y^2 \leq k^2,$$

$$k_z = -j\sqrt{k^2 - k_x^2 - k_y^2}, \text{ otherwise.} \tag{2}$$

In (2) k is the wave number, and k_x, k_y, k_z are the components of the propagation vector (or the spatial frequencies in x-, y-, and z- directions), and $E_t(x, y, z_0)$ is the tangential field (a certain component of it) on the scanning planar surface (x, y) at the elevation z_0 above the image plane (see. Figure 1). Operators $\mathcal{F}$ and $\mathcal{F}^{-1}$ represent forward and inverse 2D Fourier transform.

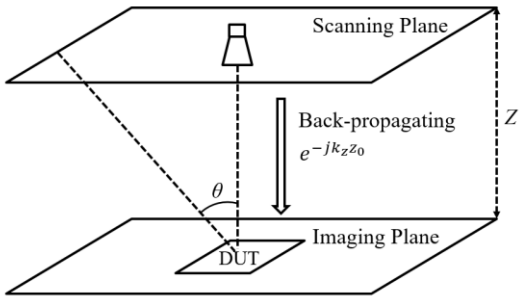

Figure 3. 2D ESM scanning arrangement.

Since the sparse ESM is carried out with non-uniformly located scanning points, a predefined grid of zero values is created before the scanning and filled-in during the scanning process [2], [4]. The signal-to-noise ratio of the image acquired with random sampling is approximately equal to the number of the sparse samples and does not depend on the density of the grid [4].

2.2. SPARSE ESM SYSTEM USING GPR

The GPR is performed separately for real and imaginary parts of the measured field distribution, and the mean values μ_{real} and μ_{imag} as well as their standard deviations σ_{real} and σ_{imag} are estimated on the sampling plane (see [8] for details). The total field power and its uncertainty are then calculated as

$$P = \mu_{real}^2 + \mu_{imag}^2 , \tag{3}$$

$$\sigma = \sqrt{\sigma_{real}^2 + \sigma_{imag}^2} . \tag{4}$$

Obviously, the regions with the largest power on the scan plane and high uncertainty in the estimated field are supposed to be scanned primarily. Therefore, the

empirical point selection criterion was developed [8] which requires the calculation of the product of the predicted field power and its uncertainty. According to it, the next measurement is performed at the location x_{n+1} (n being the number of previously acquired samples) with the maximum product of the predicted power and uncertainty. At the same time, the next measurement point should not be closer than a certain distance ε (typically a fraction of a wavelength) to already sampled ones x_i to avoid undesirable clustering effect (see [2] for details):

$$x_{n+1} = x|\max[\sigma \cdot P]$$
$$\forall\, i \in [1\,, n\,], |x_{n+1} - x_i| \geq \varepsilon. \tag{5}$$

Because of the constrain in (8), the distance between the sampling points cannot be smaller than ε, which limits the maximum number of samples in the scanning area.

3. SIMULATION AND MEASUREMENT RESULTS

3.1. SIMULATED GPR SCAN FOR A THREE-SOURCE SCENE

In the simulation of the automatic sparse ESM using Gaussian process regression, three horizontally oriented dipoles are put on the image plane at different positions. The working frequency is 6 GHz, with the wavelength λ=0.05 m, and the aperture of the scanning and image planes is 20 λ×20 λ (1×1 m^2).

The E_x (tangential) component of the field due to the dipoles was calculated on the scan plane using analytical formulas for an infinitesimal dipole [9]. The parameters of the dipoles are listed in Table 1.

Table 1. Parameters of radiation sources used in simulation.

Source	Dipole 1	Dipole 2	Dipole 3
Position (X, Y) [λ]	(-8, -8)	(8, 8)	(8, -8)
Dipole moment [A·m]	1	1	0.5

To verify the performance of the GPR method, the random sampling method is simulated as a comparison. The images obtained as the result of the ESM process are normalized to their corresponding maxima to facilitate their comparison (the absolute values of the images depend on the number of samples and the sampling density). Estimation of the absolute value of the image can be performed if needed using interpolation of the scanned field as described in [4].

To quantify the error of the obtained image the mean squared difference between the normalized images is calculated:

$$MSE_E = \frac{1}{m}\sum_{i=1}^{m}\left(\frac{|E_S(i)|}{\max|E_s|} - \frac{|E_0(i)|}{\max|E_0|}\right)^2, \quad (6)$$

where E_S is the image obtained by using the GPR or the random sampling method, E_0 is the actual image (obtained by the complete uniform scan), and m is the number of the samples in the image (i.e. on the number of the samples in the predefined grid).

As shown in Figure 2 (a), there are three dipole sources in the actual image, which is obtained by sampling the field at the scan plane at 101x101 locations on a predefined uniformly spaced grid.

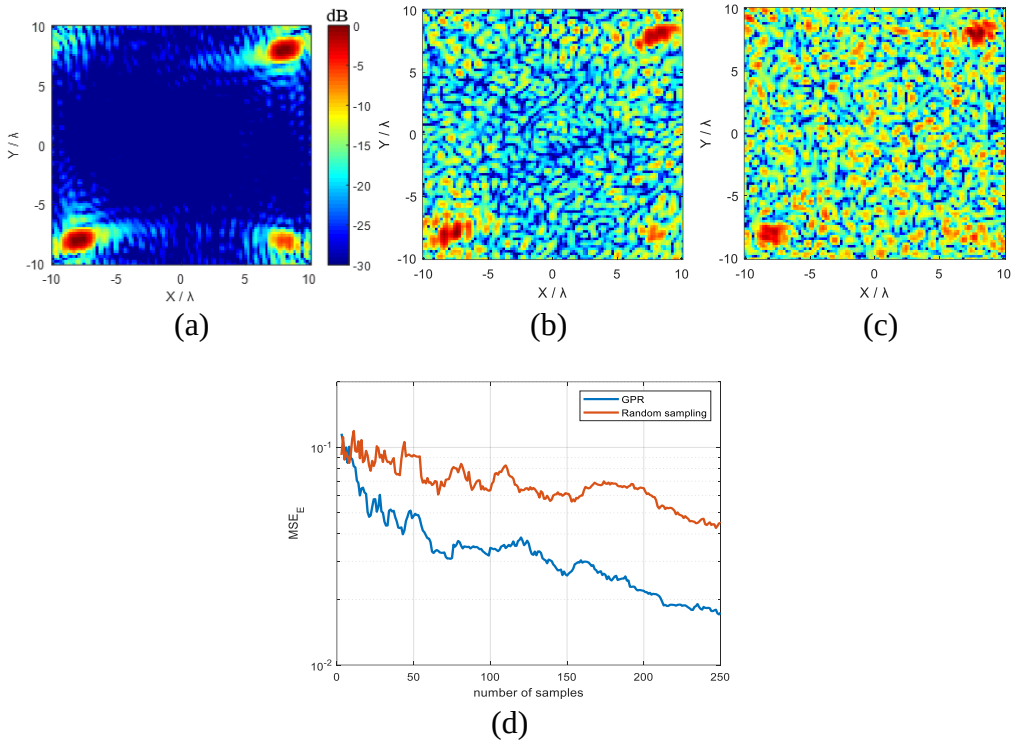

Figure 2. ESM images for the three-dipole scene obtained by uniform, GPR, and random sampling: (a) Actual image with 101×101 samples, (b) GPR ESM image with 250 samples, (c) Random ESM image with 250 samples, (d) MSE_E as a function of the number of sampling points for GPR and random sampling.

The images obtained by taking 250 samples (approximately $1/41$ of total sampling points of the actual image) randomly or by the GPR selection are shown in Figure 2 (b-c). Both GPR and random sampling can clearly resolve dipoles 1 and 2. At the same time, the noise level in the central region of random sampling image is obviously higher than that in the GPR sampling. Moreover, as can be seen, even with this relatively low number of points the GPR sampling allows to resolve the weak dipole 3 located at (8λ, -8λ) with much higher certainty compared to the random scan. The evolution of the mean squared error in the scanning process is illustrated by Figure 4(d). As can be seen, the accuracy of the GPR imaging (characterized by the corresponding

MSE value) is consistently better than that of the random sampling starting from approximately 30 acquired samples. After 250 iterations the error in the GPR imaging error is approximately 2.6 times lower than that of the random scanning process. The results in Figure 2 demonstrate the advantage of the GPR imaging over random sampling in terms of the scanning time – i.e. the ability to obtain the image of better quality for the same number of acquired samples, or to reduce the number of samples needed to obtain an image of a certain quality.

3.2. PRACTICAL IMPLEMENTATION OF THE GPR ESM SCAN

To test the method in realistic conditions, mimicking the measurement of emissions of an electronic device in a metallic chassis, two experiments, first with the passive source (a VNA-driven antenna) and then with the active IC source, were performed.

3.2.1. Metal Box Excited by A Monopole Antenna. To perform the tests in this section a modified 3D printer shown in Figure 3 is used. The available scan volume of the scanner is = 0.3m × 0.3m × 0.3m. In all following examples, the image and the scan planes are parallel horizontal planes (XY). The minimum scanning step of the automatic scanning system is approximately 0.1 mm, which is at least 10 times smaller than the wavelength up to 300 GHz. The scanning probe – a horn antenna working in the frequency band from 8 GHz to 12 GHz – is fixed to the carriage, shown by the red marker 1 in Figure 3. The carriage is moved by the step motors through two timing belts, and the scanning process is controlled by a PC.

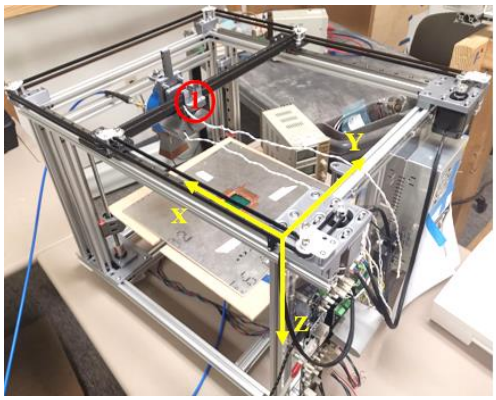

Figure 3. Automatic scanning system.

The ESM scanning system setup with the DUT is shown in detail in Figure 4 (a-c). The DUT consists of three parts: a 0.11 m × 0.19 m × 0.05 m semi-closed metal box (b), a copper lid (c), and a short monopole to excite the cavity. The copper lid is inserted into the rebate on the box walls, and the monopole driven through a coaxial connector is put on the wall of the enclosure box. The monopole excites the cavity modes in the box and the four seams between the box and the lid act as secondary sources producing electromagnetic emissions. The scanning antenna and the monopole are connected to the VNA ports as shown in Figure 4 (a).

The field on the scan plane E is related to the transmission coefficient S_{12} between the ports as

$$E = S_{12} V_2^+ A \,. \tag{7}$$

where V_2^+ is the amplitude of the outgoing wave in port 2 (the port driving the monopole), and A is the combined scanning antenna factor and cable attenuation.

Since the absolute values of the field were not of interest in this study, both V_2^+ and A are assumed to be equal to 1 V and 1 1/m respectively, and the value of S_{12} (or S_{21}

due to reciprocity) was treated as a field intensity on the scan plane scaled by an unknown coefficient.

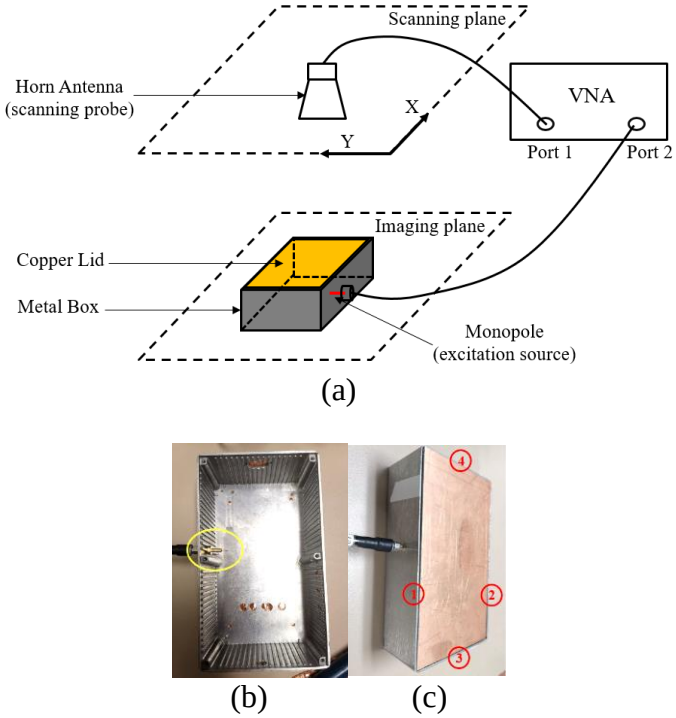

Figure 4. Measurement setup for the metal box with the monopole excitation: (a) measurement arrangement, (b) the monopole and the semi-closed metal box, (c) the copper lid and four seams.

The measurements are performed at the frequency of 8.6 GHz, which corresponds to one of the resonances of the cavity. The image plane is aligned with the copper lid, and the distance between the scan plane (defined by the scan antenna aperture) to the image plane is set to 9.5 cm. Similar to the simulated results presented in the previous section, uniform, random, and GPR sampling measurement were performed.

The scan plane aperture is 0.28 m×0.28 m. In the scanning process the predefined zero-valued array of 29x29 locations (sampling step of 1 cm, giving 3.5 samples per wavelength) is filled with the sampled field values as they are acquired.

Figure 5 (a) shows the uniform sampling ESM result, working as the reference for comparison (the black rectangle shows the outline of the metal box). Figure 5 (b-g) and (h-m) show the random and GPR sampling ESM images after different number of sampling points respectively.

As can be seen, the emissions from seams 1 and 2 are clearly visible in the reference image (the emissions from the other two seams are not detected because they are in cross-polarization with the scanning antenna) forming relatively long (distributed) features.

By analyzing the plots in Figure 5, it can be concluded that the quality of the image in the random scan grows quite slowly as the samples are added, and after taking 500 samples the amount of noise is still large and many of the image details are not visible. While in the GPR scan, the image obtained with just 250 samples is visually very similar to the reference image with all important features already present.

Similar conclusions could be made by comparing the error curves for both processes in Figure 6 – the GPR scan starts to outperform the random one from the very first samples. After 200 sampling points, the error of the GPR scan is approximately 10 dB lower than the random scan one.

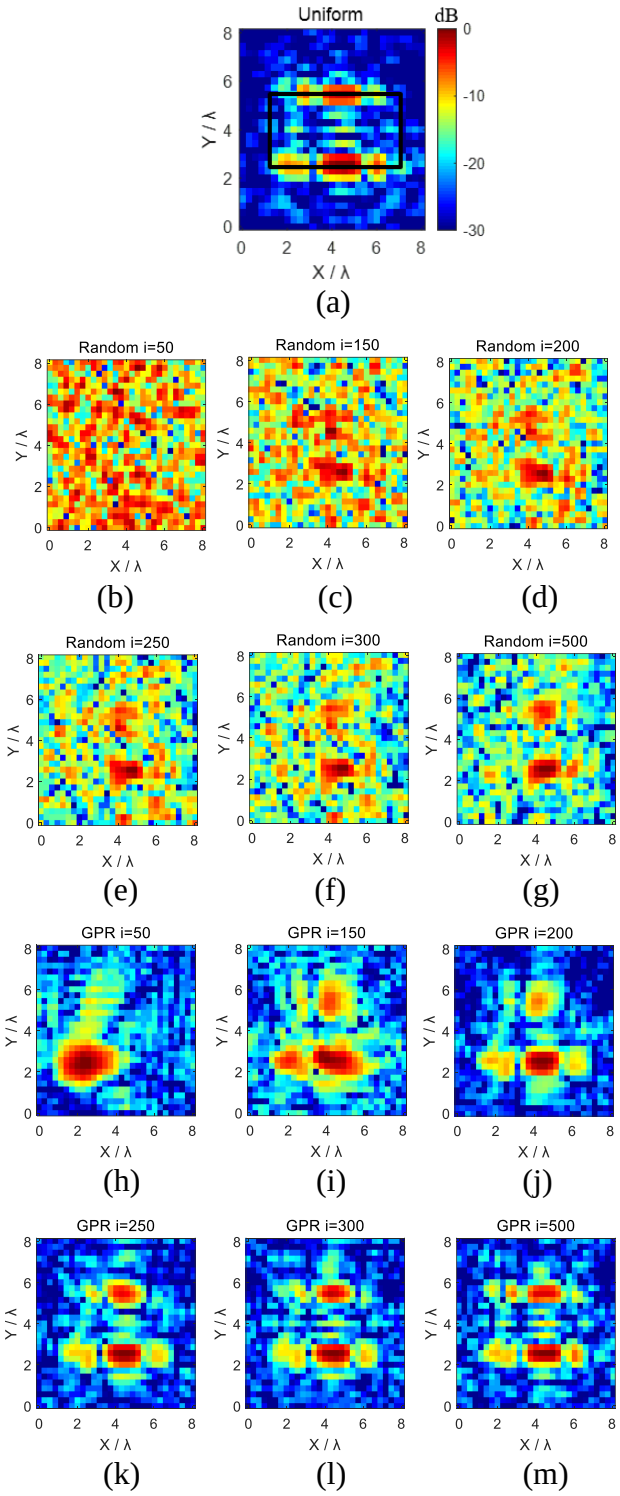

Figure 5. Uniform, random and GPR ESM images for different number of sampling points: (a) complete uniform sampling ESM image with the box outline, (b-g) random sampling ESM images after 50, 150, 200, 250, 300, 500 sampling points, (h-m) GPR ESM images after 50, 150, 200, 250, 300, 500 sampling points.

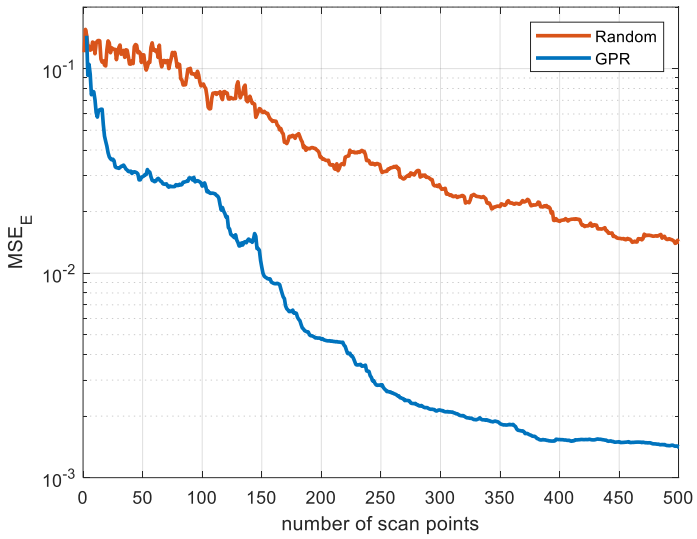

Figure 6. Comparison of the MSE_E as a function of the number of sampling points for the GPR and random sampling.

3.2.2. Electromagnetic Cavity with Active IC Excitation Source. The input signal for the IC is produced by the RF signal generator tuned to 3 GHz with 0 dBm output power. The clock buffer IC mounted on the metal plate is covered by the metal box (the same one as in the previous experiment) to mimic the chassis of an electronic device. The gap between the box and the metal plate acts as a secondary emission source.

The receiver (a VNA in the tuned receiver mode) is tuned to the third harmonic of the input signal (9 GHz). This is done to measure the emissions created by the IC itself, not by the output signal of the generator, which unavoidably leaks into the cavity and excites it. The reference signal, needed to obtain the phase of the scanned field is picked-up by the monopole antenna attached to the box and is fed to port two of the VNA by a coaxial cable.

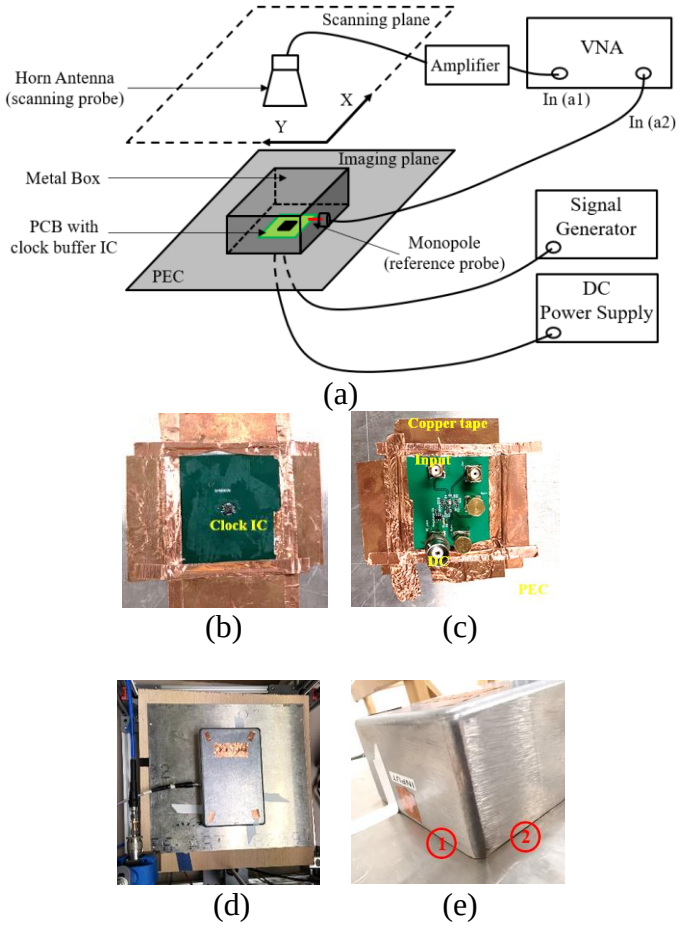

Figure 7. Measurement setup for the metal box with the active IC excitation: (a) measurement arrangement, (b) top view of the clock IC PCB, (c) botton view of the clock IC PBC, (d) view of the PEC with the metal box, (e) potential secondary emission sources.

The reference signal, needed to obtain the phase of the scanned field is picked-up by the monopole antenna attached to the box and is fed to port two of the VNA by a coaxial cable. Since the radiation produced by the IC outside of the metal box is relatively weak, the amplifier is added to channel 1 to increase the SNR. Figure 8 shows the spectrum of the signals in the scan (with the scan antenna placed over one of the short seams of the box) and reference channels around 9 GHz, showing that the SNR in both channels is above 25 dB. The complex amplitude of the scanned field is calculated (with

respect to the unknown scaling factor due to the antenna, amplifier, cables, and power of the signal in the reference channel) as

$$E = \frac{V_1}{V_2},$$

where V_1 and V_2 are the signals received in ports 1 and 2 of the VNA respectively.

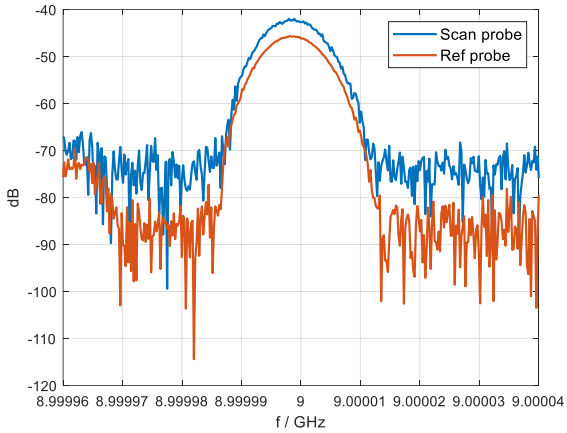

Figure 8. The spectrum of the 3rd harmonic signal received by the VNA.

The scanning process settings are identical to those in case (1); similarly, the uniform, random, and GPR sampling ESM results are shown in Figure 9 (a-m).

The evolution of the images is similar to the previous experiment. As can be seen from Figure 9 (a), the emissions from the two short seams are obvious in the uniform sampling image forming relatively long distributed features (the black rectangle shows the outline of the metal box). Similarly, analyzing all plots in Figure 9, the conclusion can be made that the image quality of random scan increases relatively slowly as the samples are added, while in the GPR scan, the image obtained after 250 iterations is already visually similar to the reference image and most relevant features are revealed.

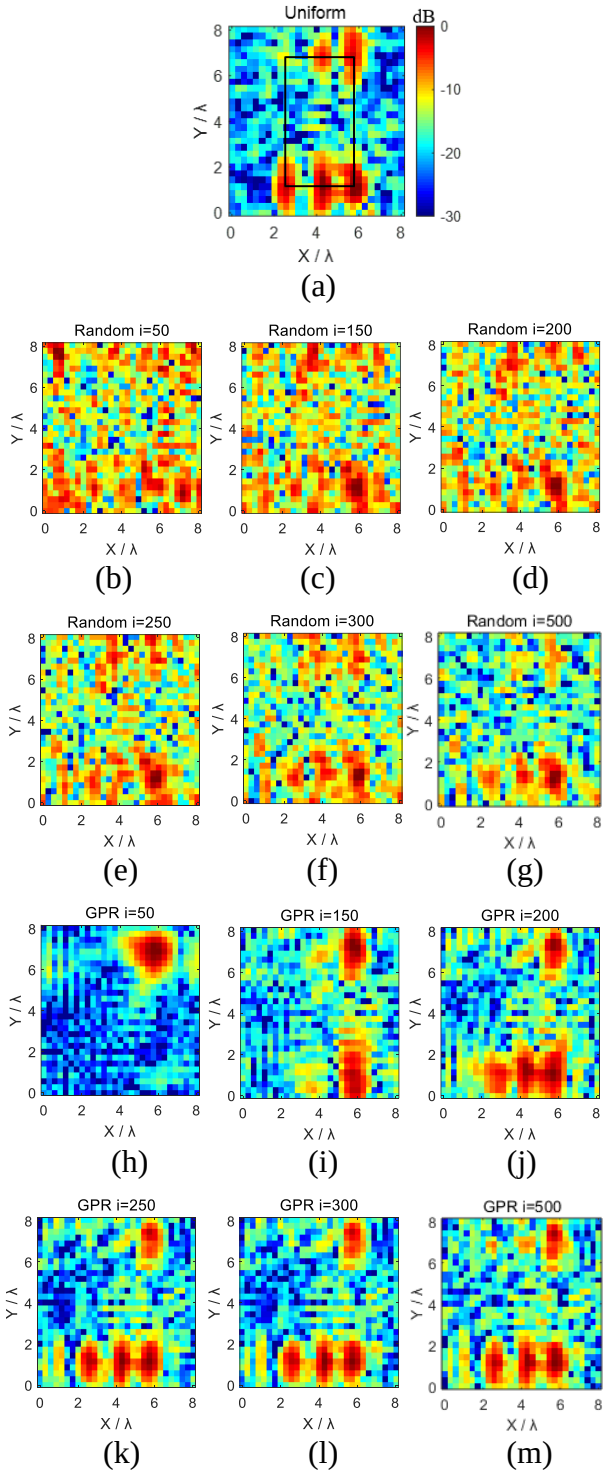

Figure 9. Uniform, random and GPR sampling ESM images for different number of sampling points: (a) complete uniform sampling ESM image with the box outline, (c-h) random sampling ESM images after 50, 150, 200, 250, 300, 500 sampling points, (i-n) GPR sampling ESM images after 50, 150, 200, 250, 300, 500 sampling points.

After taking 500 samples the amount of noise in the random scan is obviously larger than in the GPR scan, and many important details are still not visible in the random scan image. The result in Figure 10, demonstrating the evolution of the error, is consistent with this conclusion.

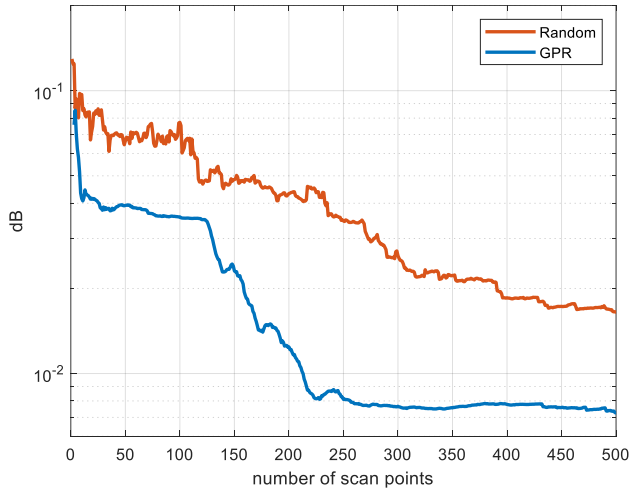

Figure 10. Comparison of the MSE_E as a function of the number of sampling points for the GPR and random sampling.

3.2.3. GPR Sampling ESM Scanning Process Analysis. To illustrate how GPR instructs the ESM system to choose the sampling points, the sampled locations as well as the magnitude of the $\boldsymbol{\sigma} \cdot \boldsymbol{P}$ value, which is used to select the next sampling location, are plotted together. Figure 11 (a-e) shows the distribution of $\boldsymbol{\sigma} \cdot \boldsymbol{P}$ along with the locations of the sampling points already taken for 50, 100, 150, 300, and 500 iterations.

At the first 100 sampling points, the GPR instructed the scanner to scan primarily over the top emission source region shown in Figure 9(a) since the region has relatively high power and uncertainty.

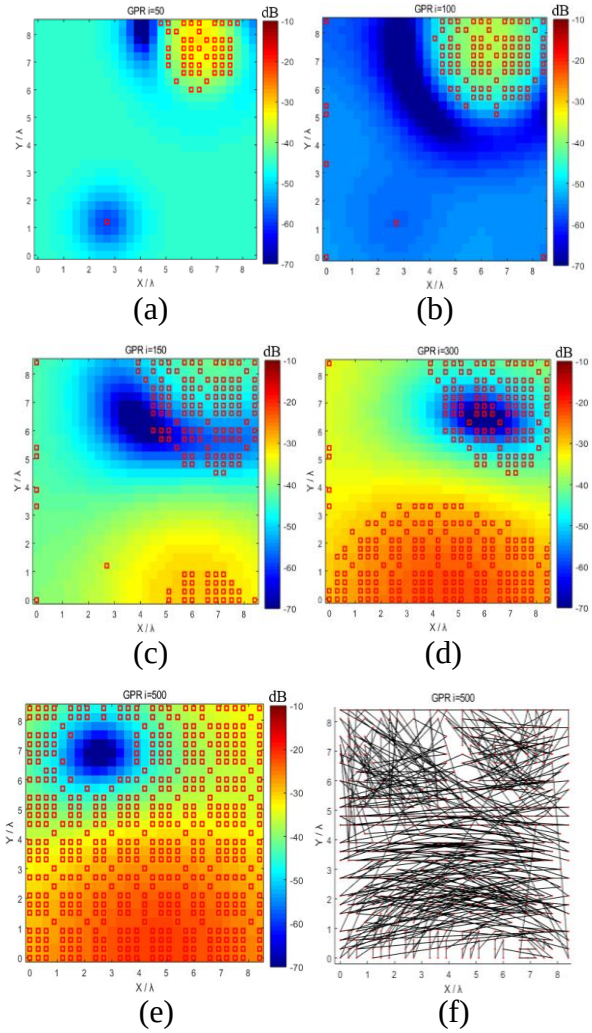

Figure 11. $\sigma \cdot P$ value distribution and sampling points pattern for the GPR scan: (a) 50th iteration, (b) 100th iteration, (c) 150th iteration, (d) 300th iteration, (e) 500th iteration, (f) scan trajectory after 500 iterations.

After that, the GPR sampling process mainly concentrated on the bottom emission source region from 150 to 300 sampling points, when the value of $\sigma \cdot P$ over this region becomes high. As shown in Figure 9 (j-m) and Figure 10, the accuracy and quality of the GPR image increases significantly during the GPR process from 150th to 300th iteration. After the 500th iteration, the GPR sampling points are almost uniformly distributed, but the blue area shown in Figure 11 (e) is still without any sampling points because of the

relatively low power of the field in that region. Finally, Figure 11 (f) shows the scan trajectory of the 500 sampling points.

4. SUMMARY

An automatic sparse ESM using Gaussian process regression method has been applied for a 2D scan of multiple distributed emission sources. Experiments mimicking the process of conducting the ESM scan over an active electronic source were conducted. Using the proposed method, the quality of the ESM imaging can be improved compared to the random scan without using an operator-controlled setup. The GPR scan allows to significantly reduce the number of samples compared to uniform and random scan due to intelligent selection of scan areas relevant for the image.

REFERENCES

[1] P. Maheshwari, H. Kajbaf, V. V. Khilkevich, and D. Pommerenke, “Emission source microscopy technique for EMI source localization,” IEEE Trans. Electromagn. Compat., vol. 58, no. 3, pp. 729–737, Jun. 2016.

[2] M. Sørensen, H. Kajbaf, V. V. Khilkevich, L. Zhang and D. Pommerenke, "Analysis of the Effect on Image Quality of Different Scanning Point Selection Methods in Sparse ESM," in IEEE Transactions on Electromagnetic Compatibility, vol. 61, no. 6, pp. 1823-1831, Dec. 2019.

[3] J. T. Case, M. T. Ghasr, and R. Zoughi, “Nonuniform manual scanning for rapid microwave nondestructive evaluation imaging,” IEEE Trans. Instrum. Meas., vol. 62, no. 5, pp. 1250–1258, May 2013.

[4] L. Zhang, V. Khilkevich and D. Pommerenke, "Sparse Emission Source Microscopy for Rapid Emission Source Imaging," in IEEE Transactions on Electromagnetic Compatibility, vol. 59, no. 2, pp. 729-738, April 2017.

[5] H. He, V. Khilkevich and D. Pommerenke, "2D imaging system with optical tracking for EMI source localization," 2015 IEEE Symposium on Electromagnetic Compatibility and Signal Integrity, Santa Clara, CA, 2015, pp. 107-110.

[6] D. Deschrijver, F. Vanhee, D. Pissoort, and T. Dhaene, “Automated near-field scanning algorithm for the EMC analysis of electronic devices,” IEEE Trans. Electromagn. Compat., vol. 54, no. 3, pp. 502-510, Jun. 2012.

[7] Singh, D. Deschrijver, D. Pissoort, and T. Dhaene, “Accurate hotspot localization by sampling the near-field pattern of electronic devices,” IEEE Trans. Electromagn. Compat., vol. 55, no. 6, pp. 1365-1368, Dec. 2013.

[8] J. Li, J. Zhou, S. Yong, Y. Liu and V. Khilkevich, "Automatic sparse ESM scan using Gaussian process regression," 2020 IEEE International Symposium on Electromagnetic Compatibility & Signal/Power Integrity (EMCSI), Reno, NV, USA, 2020, pp. 671-675, doi: 10.1109/EMCSI38923.2020.9191463.

[9] C. A. Balanis, Antenna Theory: Analysis and Design, New York:Wiley, 1982.

SECTION

2. CONCLUSIONS

An automatic sparse ESM using Gaussian process regression method has been developed. Using the proposed method, the quality of the ESM imaging can be improved compared to the random scan without using operator-controlled setup. The number of the scan points can be potentially reduced compared to uniform and random scan due to intelligent selection of scan areas relevant for the image.

Uniform ESM imaging provides the best results in terms of the image quality but leads to a long scanning time needed to sample the fields on the plane with sub-wavelength step required to satisfy the Nyquist criterion. To overcome the problem a sparse scanning strategy was proposed. With the random selection of the sampling locations, the dynamic range of the image (related to the amount of noise added due to space sampling) is equal to the number of samples. And while sparse random sampling often produces satisfactory results, it still can lead to prohibitively long scanning times needed to achieve a desirable image quality. An alternative to random sampling is manual sampling which usually provides fast scanning but requires a human operation, and the scanning process is affected by the operator's subjective decisions and perceptions. In recent years the Gaussian process regression (GPR) or Kriging interpolation was proposed as a method for fast scanning of electromagnetic fields. The GPR strategy was successfully applied to the ESM scan. This method allowed to reduce the number of samples needed to achieve a certain dynamic range of the image, reducing the overall

scanning time and eliminating a need of human intervention into the ESM process. This paper completed the application of the ESM with GPR sampling to 1D/2D scenes with multiple sources, including distributed ones.

Experiments mimicking the process of conducting the ESM scan over an active electronic source were conducted. Using the proposed method, the quality of the ESM imaging can be improved compared to the random scan without using an operator-controlled setup. The GPR scan allows to significantly reduce the number of samples compared to uniform and random scan due to intelligent selection of scan areas relevant for the image.

VITA

Jiangshuai Li received his B.E. degree in electrical and computer engineering from the Huazhong University of Science and Technology, Wuhan, China, in 2019. He worked in electrical engineering from the EMC Laboratory, Missouri University of Science and Technology (formerly University of Missouri-Rolla), Rolla, MO, USA from 2019 to 2021. His research interests included electromagnetic interference, radio frequency integrity, signal integrity in high-speed digital systems and microwave imaging. He received his master of science degree in Electrical Engineering from Missouri University of Science and Technology, USA, in May 2022.